Synthesis, Characterization, and Magnetic Studies of Coordination Polymers with Co(II) and Mn(II) Ions

ARTICLE *in* CRYSTAL GROWTH & DESIGN · SEPTEMBER 2012

Impact Factor: 4.89 · DOI: 10.1021/cg300829c

CRYSTAL GROWTH & DESIGN

Article

pubs.acs.org/crystal

Synthesis, Characterization, and Magnetic Studies of Coordination Polymers with Co(II) and Mn(II) Ions

Musheer Ahmad,[†] Raja Das,[‡] Prem Lama,[†] Pankaj Poddar,*[,‡] and Parimal K. Bharadwaj*[,†]

[†]Department of Chemistry, Indian Institute of Technology, Kanpur 208016, India

[‡]Physical & Materials Chemistry Division, National Chemical Laboratory, Pune 411 008, India

Supporting Information

ABSTRACT: An ether bridged tricarboxylic acid ligand, 5-(4-carboxybenzyloxy)-isophthalic acid (*p*-cbiaH$_3$) has been used to construct three coordination polymers with Co(II) salts in presence of different nitrogen donor ligands such as 1,4-bis(4-pyridinylmethyl)piperazine (bpmp), dipyridine-4-yl-diazene (dpd), and 4,4′-bipyridine (bpy). The products formed under hydrothermal conditions are formulated as $\{[Co_3(p\text{-cbia})_2(bpmp)_2(H_2O)_6]\cdot 10H_2O\}_n$ (**1**), $\{[Co_2(p\text{-cbiaH})_2(dpd)(H_2O)_2]\}_n$ (**2**) and $\{[Co_3(p\text{-cbia})_2(bpy)(H_2O)_8]\cdot 6H_2O\}_n$ (**3**). Reacting with $MnCl_2\cdot 4H_2O$ under solvothermal condition, it affords $\{[Mn_3(p\text{-cbia})_2(DMF)_2]\cdot DMF\}_n$ (**4**). All the complexes have been characterized by single-crystal X-ray diffraction, IR spectroscopy, thermogravimetry, elemental analysis, and powder X-ray diffraction (PXRD) measurements. Topological analysis reveals that **1** is a (3,4)-connected jeb net, **2** is a (3,8)-connected tfz-d net, while **3** forms a 3-connected hcb type net. However, with the Mn(II) salt, it forms a 3D coordination polymer with a novel (5,6,6)-connected, three nodal net with novel pkb-4 topology. Magnetic susceptibility measurements of complexes **1**, **2**, and **4** were carried out in the temperature range 2−300 K. Complex **1** exhibits weak ferromagnetic ordering at low temperature owing to the frustration of one of the Co(II) ions in the unit cell. Complex **2** shows a peak at ∼6.1 K in ZFC susceptibility, which might result from weak ferromagnetic interactions between carboxylate-bridged Co(II) ions. Complex **4** shows a signature of antiferromagnetic behavior followed by weak ferromagnetic interactions at low temperature.

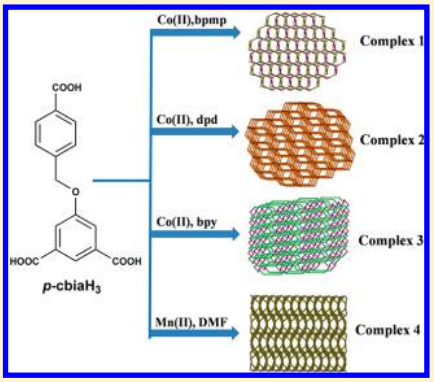

INTRODUCTION

The design and synthesis of coordination polymers (CPs) continue to attract enormous interest due to their novel architectures as well as potential applications.[1] Magnetic properties of these materials are particularly catching the imagination of chemists with an ever-growing number of CPs being reported.[2] Carboxylate-donating linkers and paramagnetic metal ions as nodes provide excellent means of achieving such magnetic materials because of versatile binding abilities of the former coupled with the capability of facile magnetic transmission.[3]

In CPs, the magnetic ordering arises from cooperative interactions between the paramagnetic centers through bridging ligands at low temperatures where the exchange energy dominates the thermal energy and stabilizes the ordering. The construction of different types of CPs with variable intermetallic distances and bond angles, besides understanding the mechanism of long-range ordering, spin frustration, meta-magnetism, anisotropy, etc., are particularly interesting.[4] The advantages CPs offer over simple inorganic complexes are the possibilities of tuning and controlling of magnetic coupling via choice of linkers and nodes.[5] It is, therefore, no surprise that a significant number of CPs exhibiting ferromagnetism,[6] antiferromagnetism,[7] spin-canting,[8] meta-magnetism,[9] single chain magnetism,[10] spin-glass behavior,[11] etc., have been synthesized and studied. Recently, CPs exhibiting both magnetic and electrical ordering (multiferroic) in a single phase were also demonstrated.[12]

We have recently exploited flexible and rigid nitrogen-based ligands as spacers in the metal carboxylate system to formulate these extended complexes.[9,13] The coordination frameworks based on rigid ancilliary ligands, such as 4,4'-bipyridine, pyrazine, phenazine, have been extensively studied due to their regular binding capabilities.[14] In contrast, pyridine-based flexible coligands, such as 4-bis(4-pyridinylmethyl)piperazine (bpmp), dipyridine-4-yl-diazene (dpd), 1,2-di(4-pyridyl)-ethylene (dpe), have not been much explored. These bridging ligands can freely rotate to meet the requirement of coordination geometries of metal ions in the assembly process. Moreover, their variable flexibility and functionality results in interesting framework properties, such as unique dimensionality, void, degree of interpenetration, and topology.

Our previously reported complexes with this ligand exhibited ferromagnetic behavior associated with mixed hydroxyl/carboxylate-bridged tetranuclear Co(II) clusters as subunits.[3] Herein, we report CPs **1**−**3** employing the same tricarboxlate ligand (Figure S13, Supporting Information) with nitrogen-based coligands and Co(II) metal ions. Structural diversity of

Received: June 19, 2012
Revised: August 2, 2012
Published: August 6, 2012

Table 1. Crystal and Structure Refinement Data for 1−4

compound	1	2	3	4
empirical formula	$C_{64}H_{90}N_8O_{30}Co_3$	$C_{21}H_{16}N_2O_8Co$	$C_{42}H_{54}N_2O_{28}Co_3$	$C_{41}H_{39}N_3O_{17}Mn_3$
formula wt	1628.24	483.29	1211.66	1010.57
cryst syst	triclinic	triclinic	triclinic	monoclinic
space group	$P\bar{1}$	$P\bar{1}$	$P\bar{1}$	$C2/c$
a, Å	9.730(7)	7.341(4)	8.280(6)	19.194(6)
b, Å	10.190(5)	9.823(6)	10.184(5)	10.022(4)
c, Å	19.529(6)	13.683(5)	15.679(4)	21.904(5)
α (deg)	78.011(5)	90.119(3)	81.102(3)	90.000
β (deg)	80.400(8)	90.245(6)	85.719(5)	90.194(5)
γ (deg)	87.705(7)	104.146(5)	74.985(6)	90.000
U, Å^3	1867.5(17)	956.8(9)	1260.8(12)	4213(3)
Z	1	2	1	4
ρ_{calc} g/cm^3	1.430	1.678	1.580	1.593
μ, mm^{-1}	0.747	0.953	1.070	0.965
F(000)	831	494	613	2068
reflns collected	10580	5263	6908	11237
independent reflns	5026	2847	3654	3138
GOF	1.030	1.031	1.051	1.120
final R indices [$I > 2\sigma(I)$]	R1 = 0.0618; wR2 = 0.1423	R1 = 0.0784; wR2 = 0.1931	R1 = 0.0593; wR2 = 0.1552	R1 = 0.0500; wR2 = 0.1206
R indices (all data)	R1 = 0.0915; wR2 = 0.1694	R1 = 0.0990; wR2 = 0.2135	R1 = 0.0809; wR2 = 0.1933	R1 = 0.0716; wR2 = 0.1600

1−**3** was observed due to differences in the flexibility and other characteristic features of the coligands used and prevailing experimental conditions. Observed magnetic properties of **1**−**2** can be attributed to their structural features, degree of nuclearity, metal−metal distances, etc., and also to their method of transmitting magnetic coupling. Complex **1** is mononuclear, exhibiting frustrated weak ferromagnetic ordering, and complex **2** shows weak ferromagnetic behavior. Additionally, complex **4** is a trinuclear manganese cluster showing mixed antiferromagnetic/ferromagnetic ordering.

EXPERIMENTAL SECTION

Materials. Reagent-grade 4-bromomethyl benzoic acid methyl ester, 5-hydroxyisophthalic acid, piperazine, 4-(chloromethyl)pyridine hydrochloride, pyridine-4-yl-amine, 4,4′-bipyridine (bpy), cobalt chloride, cobalt acetate, and manganese chloride were acquired from Aldrich and used as received. Acetonitrile (MeCN), *N*,*N*′-dimethylformamide (DMF), NaOH, and K_2CO_3 were procured from S. D. Fine Chemicals, India, and were purified prior to use.

Infrared spectra were obtained (KBr disk, 400−4000 cm^{-1}) on a Perkin-Elmer model 1320 spectrometer. Thermogravimetric analyses (TGA) were recorded on a Mettler Toledo Star system (heating rate of 5 °C/min). Microanalyses for the compounds were obtained using a CE-440 elemental analyzer (Exeter Analytical Inc.). Powder X-ray diffraction (Cu Kα radiation, scan rate 3°/min, 293 K) was performed on a Bruker D8 Advance series 2 powder X-ray diffractometer.

Magnetic Measurements. All magnetic measurements were carried out on polycrystalline samples using a SQUID VSM dc magnetometer of Magnetic Property Measurement System (PPMS) from Quantum Design Inc., San Diego, CA, USA, equipped with a 7 T superconducting magnet. The magnetic signal from the sample holder was negligible to affect our data accuracy. Corrections are based on subtracting the sample-holder signal and diamagnetic corrections estimated from Pascal constants.[15] DC magnetization M vs T curves were taken at 500 Oe field in field-cooled (FC) and zero-field-cooled (ZFC) modes with heating/cooling rate of 2 K per minute. Magnetization vs field loops were taken in a field sweep from −50 to +50 kOe at the rate of 50 Oe/s.

Single-Crystal X-ray Studies. Single-crystal X-ray data on **1**−**4** were collected at 100 K on a Bruker SMART APEX CCD diffractometer using graphite-monochromated Mo Kα radiation (λ = 0.71073 Å). For each compound, the data corrections, data integration, and reduction were carried out as described earlier.[16−19] The structure was solved by direct methods using SHELXTL-97[20] and refined on F^2 by full-matrix least-squares using the SHELXL-97 program[21] package. All non-hydrogen atoms were refined anisotropically. The hydrogen atoms attached to carbon atoms were positioned geometrically and treated as riding atoms using SHELXL default parameters. The hydrogen atoms of coordinated water molecules in **1**−**3** were located from difference Fourier maps. The hydrogen atoms of lattice water molecules could not be located in the difference Fourier maps in **1** and **3**. Several DFIX and DANG commands were used to fix the bond distances of metal-coordinated and lattice water molecules. The crystal and refinement data are collected in Table 1 while selective bond distances and angles are given in Table S1, Supporting Information.

Synthesis of the Ligands. 1,4-Bis(4-pyridinylmethyl)piperazine (bpmp), 5-(4-carboxybenzyloxy)isophthalic acid (*p*-cbiaH$_3$), and dipyridine-4-yl-diazene (dpd) were synthesized using earlier reported procedures.[22,3]

{[Co$_3$(*p*-cbia)$_2$(bpmp)$_2$(H$_2$O)$_6$]·10H$_2$O}$_n$ (1). A mixture containing *p*-cbiaH$_3$ (0.02 g, 0.06 mmol), Co(CH$_3$COO)$_2$·4H$_2$O (0.07 g, 0.39 mmol), and bpmp (0.015 g, 0.06 mmol) in 3 mL of water and 0.1 mL of 1 M NaOH solution were sealed in a Teflon-lined autoclave and heated under autogenous pressure to 130 °C for 2 days and then allowed to cool to room temperature at the rate of 1 °C/min. Block-shaped pink crystals of **1** were collected in ∼56% yield. The crystals were repeatedly washed with water followed by acetone and air-dried. Anal. Calcd for $C_{64}H_{90}Co_3N_8O_{30}$: C, 47.20; H, 5.57; N, 6.88%. Found: C, 46.61; H, 5.29; N, 6.24%. IR (cm^{-1}): 3452(m), 1606(s), 1566(s), 1455(m), 1404(s), 1369(s), 1313(m), 1260(m), 1033(s), 902(w), 873(m), 823(m), 772(s), 713(s).

{[Co$_2$(*p*-cbiaH)$_2$(dpd)(H$_2$O)$_2$]}$_n$ (2). A mixture containing *p*-cbiaH$_3$ (0.02 g, 0.06 mmol), CoCl$_2$·6H$_2$O (0.18 g, 0.77 mmol), and dpd (0.01 g, 0.05 mmol) in 3 mL of water and 0.1 mL of 1 M NaOH solution were sealed in a Teflon-lined autoclave and heated under autogenous pressure to 180 °C for 3 days and then allowed to cool to room temperature at the rate of 1 °C/min. Block-shaped pink crystals of **2** were collected in ∼60% yield. The crystals were repeatedly washed with water followed by acetone and air-dried. Anal. Calcd for $C_{21}H_{16}CoN_2O_8$: C, 52.18; H, 3.33; N, 5.79%. Found: C, 51.95; H, 3.21; N, 5.93%. IR (cm^{-1}): 3386(s), 2927(w), 1704(m), 1615(m), 1550(s), 1462(w), 1376(s), 1320(w), 1265(m), 1225(m), 1175(w), 1128(s), 1104(m), 805(m), 779(s), 716(s).

{[Co$_3$(*p*-cbia)$_2$(bpy)(H$_2$O)$_8$]·6H$_2$O}$_n$ (3). A mixture containing *p*-cbiaH$_3$ (0.02 g, 0.06 mmol), Co(CH$_3$COO)$_2$·4H$_2$O (0.07 g, 0.39

dx.doi.org/10.1021/cg300829c | Cryst. Growth Des. 2012, 12, 4624−4632

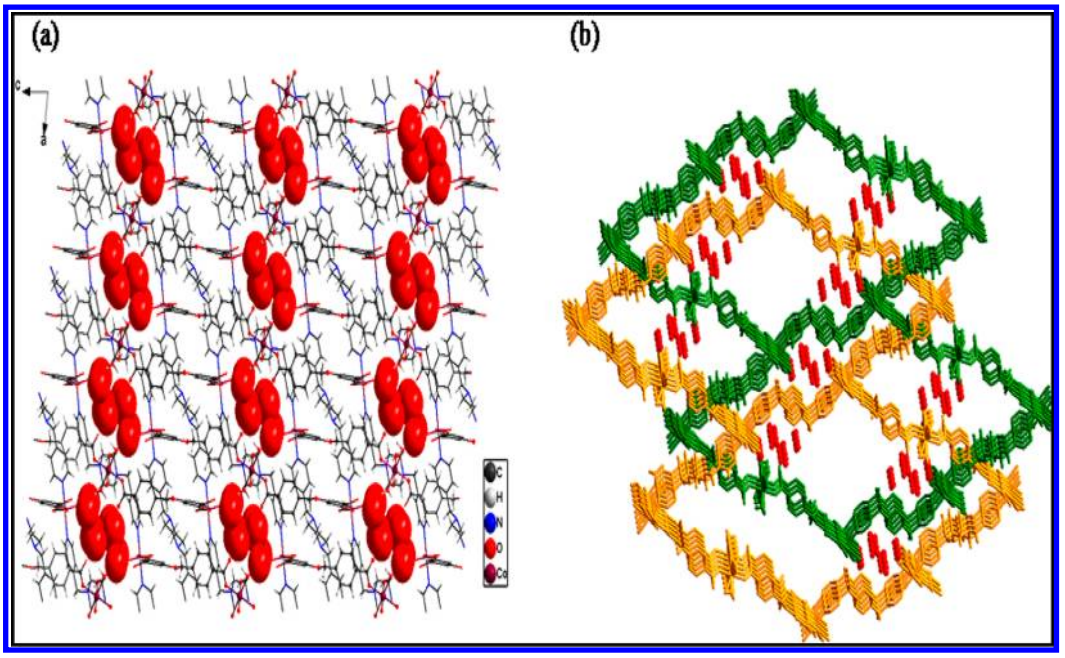

Figure 1. (a) Three-dimensional view along the *b*-axis in **1** showing lattice water molecules in space-fill model and (b) representation of interpenetration of frameworks.

mmol), and bpy (0.015 g, 0.09 mmol) in 3 mL of water and 0.1 mL of 1 M NaOH solution were sealed in a Teflon-lined autoclave and heated under autogenous pressure to 180 °C for 3 days and then allowed to cool to room temperature at the rate of 1 °C/min. Block-shaped pink crystals of **3** were collected in ∼40% yield. The crystals were repeatedly washed with water followed by acetone and air-dried. Anal. Calcd for $C_{42}H_{54}Co_3N_2O_{28}$: C, 41.63; H, 4.49; N, 2.31%. Found: C, 40.67; H, 4.21; N, 2.08%. IR (cm^{-1}): 3411(m), 3411(s), 1609(s), 1585(s), 1545(s), 1488(w), 1455(s), 1415(m), 1390(s), 1319(m), 1264(w), 1176(m), 1130(m), 1106(m), 811(s), 780(s), 724(s).

{[Mn_3(*p*-cbia)$_2$(DMF)$_2$]·DMF}$_n$ (4). A mixture containing *p*-cbiaH_3 (0.02 g, 0.06 mmol) and $MnCl_2·4H_2O$ (0.07 g, 0.28 mmol) in 1.5 mL of water, 2.5 mL of *N*,*N*′-dimethylformamide (DMF), and 0.1 mL of 1 M NaOH solution were sealed in a Teflon-lined autoclave and heated under autogenous pressure to 100 °C for 2 days and then allowed to cool to room temperature at the rate of 1 °C/min. Block-shaped colorless crystals of **4** were collected in ∼60% yield. The crystals were repeatedly washed with water followed by acetone and air-dried. Anal. Calcd for $C_{41}H_{39}Mn_3N_3O_{17}$: C, 48.72; H, 3.88; N, 4.15%. Found: C, 48.21; H, 3.71; N, 4.04%. IR (cm^{-1}): 3422(m), 2934(m), 1677(s), 1650(s), 1596(m), 1572(m), 1536(s), 1454(m), 1384(s), 1318(m), 1265(s), 1112(m), 1086(s), 852(w), 774(s).

RESULTS AND DISCUSSION

All the coordination polymers, once isolated, are stable in air and insoluble in common organic solvents and water. The IR spectra of **1**−**4** show strong absorption bands between 1408 and 1650 cm^{-1} that are diagnostic[23] of coordinated carboxylate groups.[24] The broad peak at ∼3390−3450 cm^{-1} in case of **1**−**3** indicates[25] the presence of both coordinated and non-coordinated water molecules. Complex **2** shows a broad hump at ∼2400−3100 cm^{-1}, which is the signature of protonated carboxylic group. In the case of complex **4**, the peaks around 1650 and 1677 cm^{-1} suggest the presence of coordinated and lattice DMF molecules, respectively.

Structural Description. Complex **1** crystallizes in the triclinic space group $P\bar{1}$. Here, the asymmetric unit consists of two crystallographically independent Co(II) ions (one having full occupancy and a second one with half occupancy), one *p*-cbia^{3-}, one bpmp ligand, and three coordinated and five lattice water molecules. Three carboxylate groups of the *p*-cbia^{3-} ligand bind the metal ions as μ_3-η^1:η^1:η^1:η^0:η^1:η^0 modes, both chelating and bridging (Figure S14a, Supporting Information).

Co1 shows distorted octahedral CoN_2O_4 coordination from two different carboxylate of *p*-cbia^{3-} in chelating and bridging fashion (Co−O = 2.036(3)−2.180(3) Å), one coordinated water molecule (Co−O = 2.076(3) Å), and two nitrogen atoms from two different bpmp ligands (Co−N = 2.152(4)−2.155(4) Å) (Figure S15a, Supporting Information). The Co2 has a distorted octahedral CoO_6 coordination by two oxygen atoms (Co−O = 2.070(3) Å) from two bridging carboxylate and four oxygen atoms (Co−O = 2.093(3)−2.150(3) Å) from four coordinated water molecules (Figure S15b, Supporting Information). All the Co−O and Co−N bond distances are within the range reported for octahedral Co(II) complexes.[26]

The structure is extended to an overall 3D CP via both *p*-cbia^{3-} and bpmp ligands (Figure 1). Topological analysis shows that it is a 3D CP with two 2-fold interpenetrated networks that further interpenetrate leading to an overall 4-fold interpenetrating structure consisting of (3,4)-connected jeb net with point symbol $\{6^3\}\{6^5.8\}$ (Figure 2). The water molecule OW1 that is coordinated to Co1 forms a strong H-bonding interaction with OW7 in the lattice (OW1···OW7 = 2.759(4) Å). The remaining three water molecules (OW4, OW5, and OW8) present in the cavity are also stabilized by strong H-bonding interactions (OW5···OW3 = 2.725(5) Å, OW5···OW4 = 2.734(4) Å, and OW7···OW8 = 2.758(6) Å). In addition, OW1 and OW4 form H-bonding interactions with O2 of the ligand *p*-cbia^{3-} generating a zigzag water chain (Figure 3).

Complex **2** also crystallizes in the triclinic space group $P\bar{1}$ where the asymmetric unit consists of one Co(II) ion, one *p*-cbiaH^{2-}, a half of dpd, and one coordinated water molecule. In this case, the two carboxylates of the ligand *p*-cbiaH^{2-} bind the metal ions in μ_4-η^2:η^0:η^1:η^1:η^0:η^0 modes (Figure S14b, Supporting Information). The metal ion shows distorted octahedral coordination ($CoNO_5$) from four carboxylate of

dx.doi.org/10.1021/cg300829c | *Cryst. Growth Des.* 2012, 12, 4624−4632

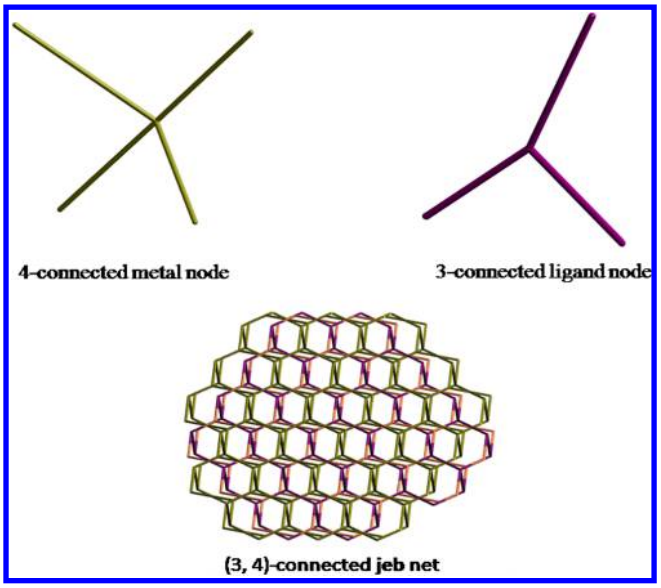

Figure 2. Topological view of (3, 4) connected net in **1**.

the ligand *p*-cbiaH^{2-} in bridging fashion (Co−O = 2.045(4)−2.182(4) Å), one coordinated water molecule (Co−O = 2.111(4) Å), and one nitrogen atom from the dpd ligand (Co−N = 2.153(5) Å) (Figure S16, Supporting Information). One of the carboxylate groups of the ligand remains protonated and noncoordinated. All the Co−O and Co−N bond distances are within the range reported for octahedral Co(II) based CPs.[26]

Interestingly, complex **2** consists of alternating double O−C−O and double O-bridges in which metal···metal distances are 4.212 and 3.315 Å, respectively (Figure 4). Further, the dimeric units are connected to the N atoms of dpd ligands, which act as pillars for the adjacent layers to generate an overall 3D framework (Figure 5). Topologically, the Co(II) ion is considered as an eight-connected node, while each *p*-cbiaH^{2-} ligand is a three-connected linker. On the basis of this simplification, **2** has a 3D noninterpenetrated (3,8)-connected tfz-d net (Figure 6). The extended point symbol for this network is $\{4^3\}_2\{4^6.6^{18}.8^4\}$.

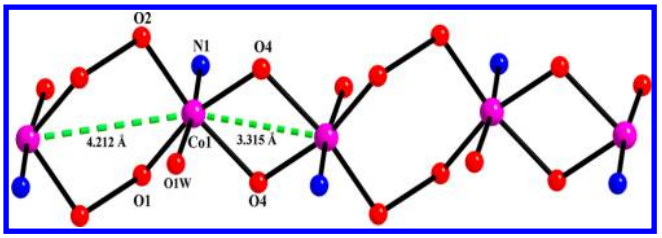

Figure 4. Representation of Co(II) chain in complex **2**.

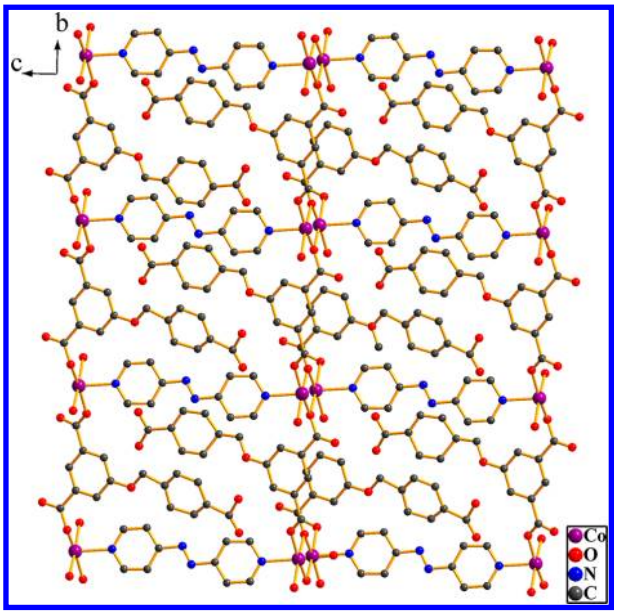

Figure 5. Three-dimensional view along the *a*-axis in **2**.

Complex **3** also crystallizes in the triclinic space group $P\bar{1}$. Here, the asymmetric unit consists of two crystallographically independent Co(II) ions (one having full occupancy and the other a half occupancy), one *p*-cbia^{3-}, a half bpy, and four coordinated and three lattice water molecules. In this case, the three carboxylate groups of the ligand bind the metal ions in μ_3-η^1:η^1:η^1:η^0:η^1:η^0 modes, both chelating and bridging (Figure

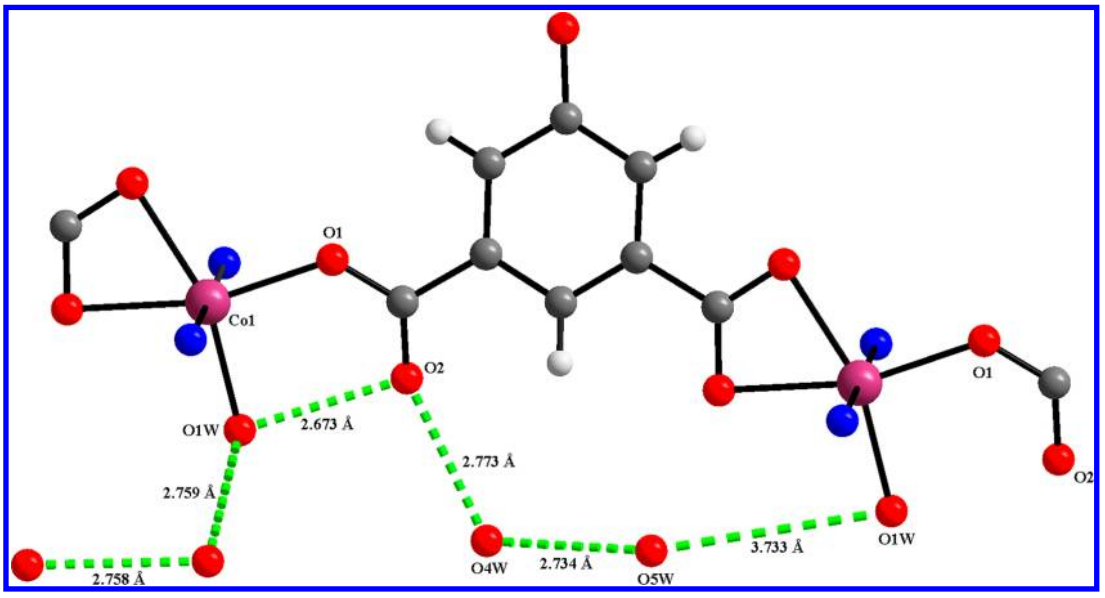

Figure 3. Water chain supported by carboxylate oxygen in **1**.

dx.doi.org/10.1021/cg300829c | *Cryst. Growth Des.* 2012, 12, 4624−4632

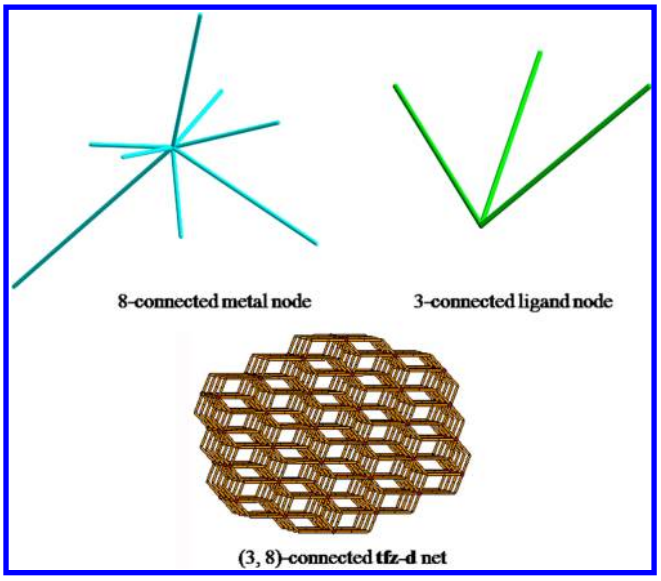

Figure 6. Topological view of (3,8)-connected net in **2**.

S14a, Supporting Information). Co1 shows distorted octahedral $CoNO_5$ coordination with ligation from two different carboxylates of *p*-cbia^{3-} ligands in chelating and bridging fashion (Co−O = 2.028(3)−2.168(3) Å), two water molecules (Co−O = 2.072(4)−2.128(3) Å), and one nitrogen atom from a bpy ligand (Co−N = 2.136(4) Å) (Figure S17a, Supporting Information). The Co2 has a distorted octahedral CoO_6 coordination from two oxygen atoms (Co2−O = 2.079(3) Å) from two bridging carboxylate and four oxygen atoms (Co2−O = 2.043(3)−2.117(3) Å) from four water molecules (Figure S17b, Supporting Information). All the Co−O and Co−N bond distances are within the range reported for Co(II)-based coordination polymers.[26]

Both *p*-cbia^{3-} and bpy ligands extend the structure to a 2D sheet (Figure 7). These 2D sheets are further interpenetrated leading to an overall 3D architecture (Figure S18, Supporting Information). The 3D polymer is further stabilized by H-bonding interactions among coordinated water molecules,

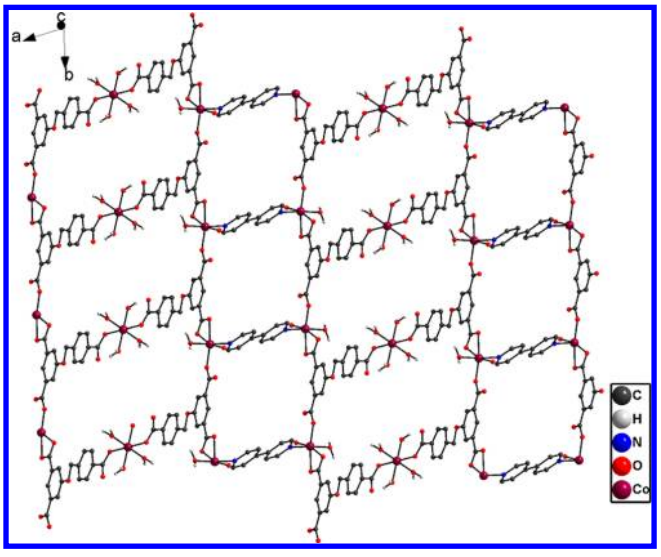

Figure 7. Two-dimensional sheet formed by *p*-cbia^{3-} and bpy ligand along the *ab* plane.

lattice water molecules, and carboxylate groups of the ligands. Topological analysis of **3** shows that the framework is a three-connected uninodal hcb type net with point symbol 6^3 (Figure 8).

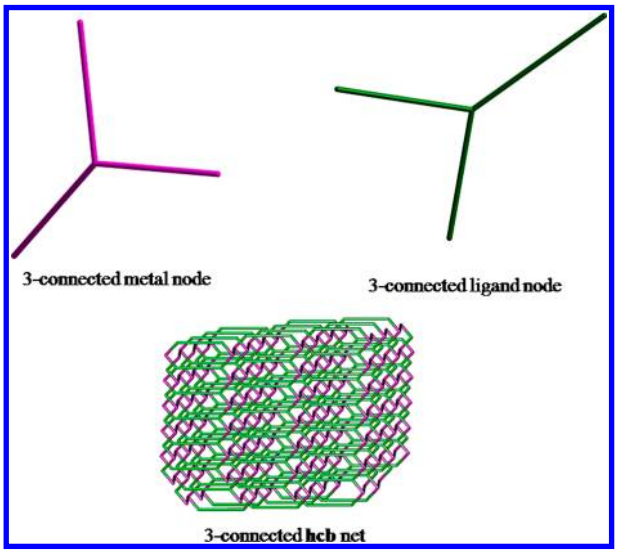

Figure 8. Topological view of three-connected net in **3**.

In contrast to the previous three structures, complex **4** was synthesized solvothermally in the absence of any pyridine-based coligand. It crystallizes in the monoclinic space group *C*2/*c* where the asymmetric unit consists of two Mn(II) ions (one having full occupancy and the second one a half occupancy), one *p*-cbia^{3-}, and one coordinated and a half lattice DMF molecule. Here, the three carboxylate groups of the ligand bind the metal ions in μ_7-η^2:η^1:η^1:η^1:η^1:η^1 modes (Figure S14c, Supporting Information). The MnO_5 pentacoordination in Mn1 is provided by the four bridging oxygen atoms from four different *p*-cbia^{3-} ligands (Mn−O = 2.097(3)−2.144(3) Å) and one coordinated DMF molecule (Mn−O = 2.288(3) Å). Mn2 shows MnO_6 distorted octahedral coordination from four bridging oxygen atoms from four different *p*-cbia^{3-} ligands (Mn−O = 2.107(3)−2.120(2) Å) and two coordinated DMF molecules (Mn−O8 = 2.277(3) Å) (Figure S19, Supporting Information). The Mn1 and Mn2 ions form a linear carboxylate-bridged chain where the metal−metal distances vary from 3.603(9) to 3.835(6) Å (Figure 9).

All the Mn−O and Mn−N bond distances are within the range reported for Mn(II)-based coordination polymers.[27] The Mn(II) chain present in the structure is further extended by *p*-cbia^{3-} ligands to an overall 3D structure (Figure 10). If each *p*-cbia^{3-} ligand is considered as a six-connected node, each Mn1 atom is considered as a five-connected node, and each Mn2 is considered as six-connected node, the overall structure of complex **4** is an extended 3D (5,6,6)-connected network. Topology analysis of **4** using the Topos software[28] indicates that it can be described as a novel (5,6,6)-connected pkb4 topology (Figure 11). The extended point symbol for this network is $\{3^2.4^3.5.6^4\}_2\{3^2.4^3.5^3.6^5.7^2\}_2\{3^4.4^4.5^4.6^3\}$.

TGA Studies. Thermal stabilities of all four complexes were examined.[24] Complex **1** shows weight loss of ∼17.7% in the temperature range of 80−110 °C that corresponds to loss of six coordinated and ten lattice water molecules. Decomposition of the complex is accomplished only above 350 °C. Complex **2** exhibit a weight loss of ∼3.2% in the temperature range of 80−

dx.doi.org/10.1021/cg300829c | *Cryst. Growth Des.* 2012, 12, 4624−4632

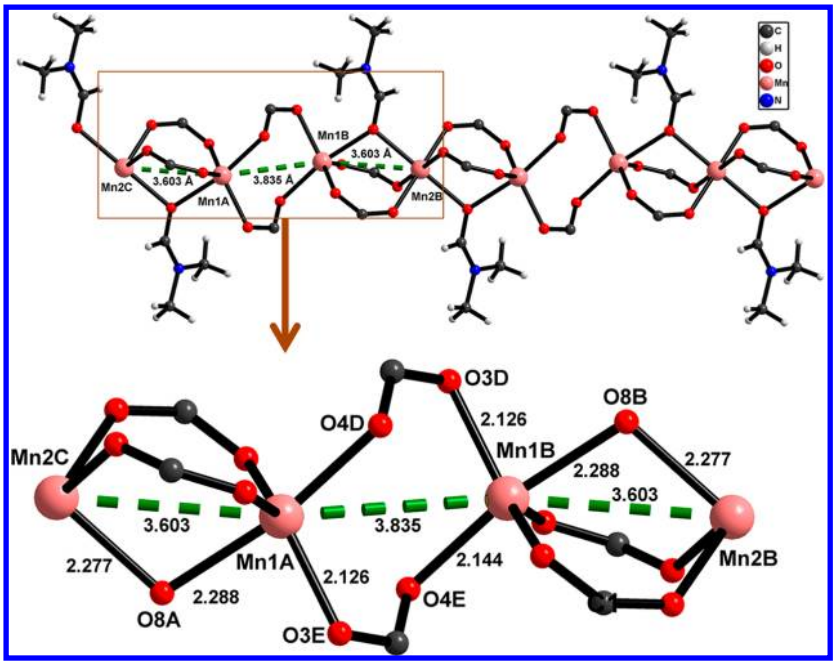

Figure 9. Metal chain generated by carboxylate units and along with DMF molecules in **4**.

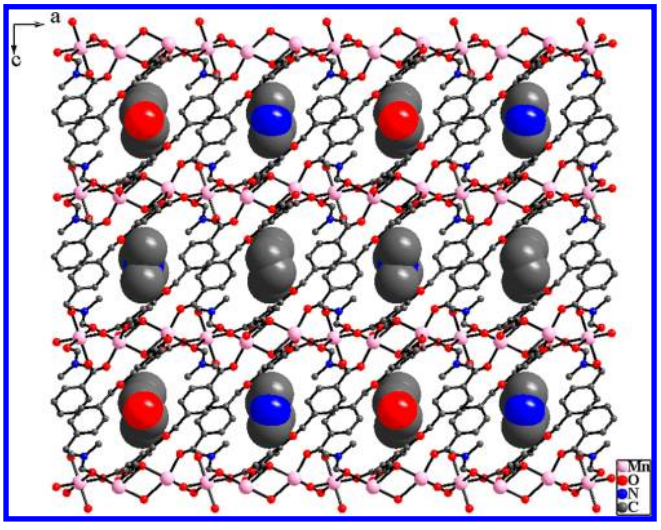

Figure 10. Three-dimensional view along the *c*-axis with lattice DMF molecules in space-filling model.

100 °C that corresponds to loss of two coordinated water molecules. Decomposition of complex **2** takes place only above 400 °C. Complex **3** shows a weight loss of ∼20.8% in the temperature range of 80−110 °C that corresponds to loss of eight coordinated and six lattice water molecules. Complex **4** exhibits a weight loss of ∼21.8% in the temperature range of 250−350 °C that corresponds to loss of two coordinated and one lattice DMF molecules. Gradual decomposition of complex **4** takes place only above 350 °C.

PXRD Analysis. Powder X-ray diffraction (PXRD) patterns of complexes **1**−**4** were in excellent agreement with the simulated patterns. The observed differences in intensity could be due to preferred orientation of the powder samples (Supporting Information, Figures S9−S12).

Magnetic Studies. *{[Co_3(p-cbia)$_2$(bpmp)$_2$(H_2O)$_6$]·10H_2O}$_n$ (**1**).* The χT value for three Co(II) ions at 300 K is 9.94 emu K mol^{-1}, which is much higher than the spin only value of 5.6 emu K mol^{-1} for three Co(II) ions with spin value 3/2 and Lande *g* value 2. This could be due to a possible orbital contribution. The χT value decreases sharply until the lowest measured temperature, 2 K. The decrease of χT could be due to the antiferromagnetic interaction between the Co(II) ions.

Below 300 K, the FC and ZFC $\chi-T$ curves show a gradual increase (typical paramagnetic behavior) and show no clear order−disorder transition until the lowest measured temperature (Figure 12). A closer look at the $M-H$ curves shows that at 50 K, complex **1** shows a linear behavior, which again indicates the typical paramagnetic behavior; however at 2 K, we see a significant nonlinear behavior with almost zero coercivity. The nonlinear behavior clearly indicates an extremely weak ordering (which could not be detected in the ZFC−FC curves). Overall, it seems that the due to competing superexchange pathways at varying temperature and the role of magneto-crystalline anisotropy, thermal energy, and Zeeman energy, the magnetic behavior shows a weak high-temperature antiferromagnetic character followed by a mixture of weak antiferromagnetic and ferromagnetic ordering at lower temperature with an absence of any clear transition temperature due to extremely weak nature of this interaction.

*{[Co_2(p-cbiaH)$_2$(dpd)(H_2O)$_2$]}$_n$ (**2**).* The temperature dependence of magnetic susceptibility for complex **2** shows quite interesting behavior as depicted in Figure 13a. The χT value for Co(II) of **2** at 300 K is 5.02 emu K mol^{-1}, which is higher than the spin only value of 1.87 emu K mol^{-1} for Co(II) ions with spin value 3/2 and Lande *g* value 2. This could be due to a possible orbital contribution. Upon cooling, the χT value decreases sharply reaches a minimum 1.00 emu K mol^{-1} at ∼14 K. Below this temperature, this value increases to a peak value of 1.78 emu K mol^{-11} at ∼8.8 K followed by a sharp drop and shows a minimum value of 0.56 emu K mol^{-1} at 2 K. The decrease of χT until 14 K could be due to the weak antiferromagnetic interaction of the Co(II) ions, which remains featureless from 14 to 300 K. However, the ZFC−FC curves show a broad hump in 20−50 K range, which is a signature of antiferromagnetic interaction between the Co(II) ions.

dx.doi.org/10.1021/cg300829c | *Cryst. Growth Des.* 2012, 12, 4624−4632

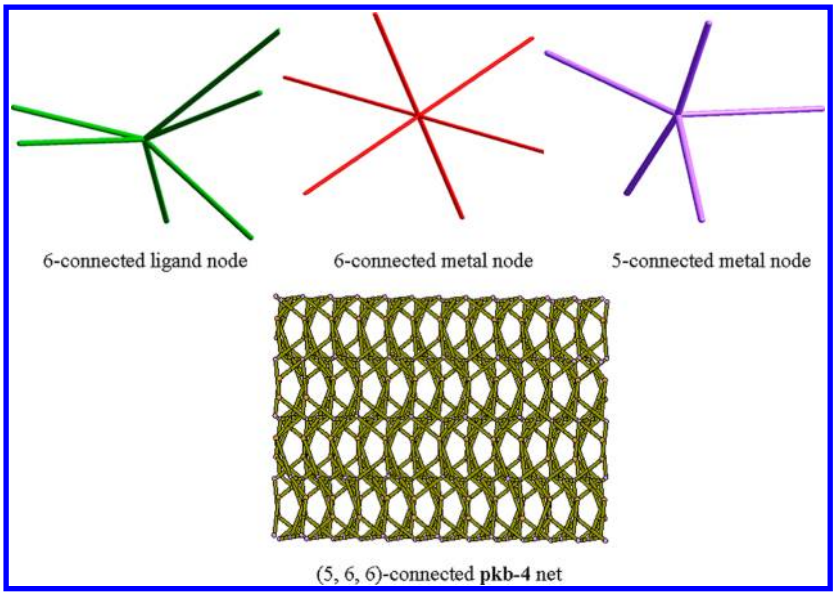

Figure 11. Structure showing (5,6,6)-connected pkb4 net in **4**.

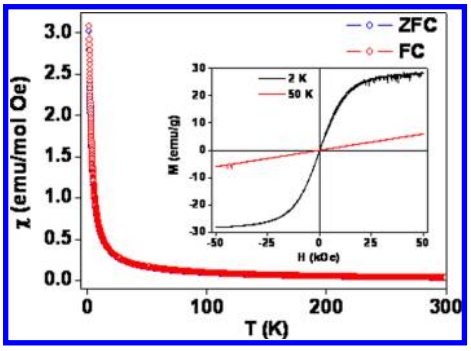

Figure 12. The temperature dependence of the magnetic susceptibility, χ, for **1** at 500 Oe applied field. MH loops taken at temperatures 2 and 50 K for **1** (inset).

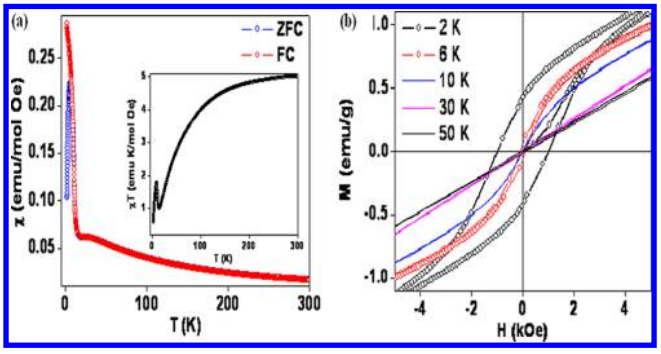

Figure 13. (a) The temperature dependence of the magnetic susceptibility χ (inset temperature dependence of the χT) for **2** at 500 Oe applied field and (b) $M-H$ loops in low-field region taken at temperatures 2, 6, 10, 30, and 50 K for **2**.

However, a sharp increase in the χT value below 14 K indicates a clear transition from a state that had an extremely weak antiferromagnetic ordering to a state where the ferromagnetic superexchange interaction dominates. The weak ferromagnetism may come from interaction between Co(II) ions having distance 3.32 Å. Below, 8.8 K, we observe a sharp bifurcation of ZFC−FC curves where the FC curve shows an increasing trend whereas the ZFC curve shows a maximum at 6.1 K and further drops until the lowest measured temperature. The splitting of the ZFC−FC curves shows the competing roles of thermal energy, magnetization energy, and anisotropy energy in the region of dominant ferromagnetic interaction below ∼14 K.

The $M-H$ curves of complex **2** are also consistent with the behavior observed in ZFC−FC $\chi-T$ curves discussed in the earlier section. At 30 and 50 K, we see a linear response, but at around 10 K a nonlinearity in the $M-H$ curve appears with almost zero coercivity, and at 6 K, this nonlinearity increases with opening up of the hysteresis loop with coercivity going up to ∼102 Oe. However, at 2 K, the $M-H$ curve shows a larger coercivity of around 984 Oe (Figure 13b). This behavior is probably due to the reduced thermal energy in comparison to the magnetocrystalline anisotropy energy below 6 K, which is consistent with observation of strong bifurcation in ZFC−FC temperature below 6.6 K. This behavior is quite similar to the magnetic behavior of superparamanetic systems below the blocking temperature.

*{[Mn_3(p-cbia)$_2$(DMF)$_2$]·DMF}$_n$ (**4**).* The temperature dependence of magnetic susceptibility for complex **4** is shown in Figure 14a. The χT value for three Mn(II) at 300 K is 13.42 emu K mol^{-1}, which is almost equal to the spin-only value of 13.125 emu K mol^{-1} for three Mn(II) ions with spin value 5/2

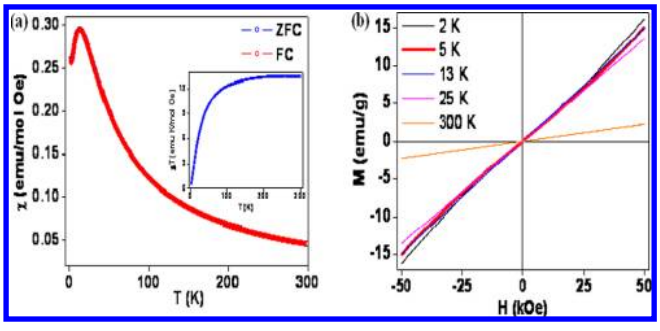

Figure 14. (a) The temperature dependence of the magnetic susceptibility χ (inset temperature dependence χT) for **4** at 500 Oe applied field and (b) $M-H$ loops taken at temperatures 2, 5, 13, 25, and 300 K for **4**.

dx.doi.org/10.1021/cg300829c | *Cryst. Growth Des.* 2012, 12, 4624−4632

and Landé g value of 2. Upon cooling, the χT value remains almost constant down to ~200 K. Below 200 K, the χT value decreases sharply to reach a minimum of 0.52 emu K mol^{-1} at the lowest measured temperature, 2 K. The decrease of χT below 200 K could be due to a weak antiferromagnetic type interaction between Mn(II) ions. The FC and ZFC $\chi-T$ curves overlap over each other. However, the FC−ZFC susceptibility curves show a peak at around 13 K below which the susceptibility value decreases until 3 K and again shows an increase in the values. The peak at 13 K in both ZFC and FC susceptibility curves indicates occurrence of another weak transition possibly antiferromagnetic in nature to the Mn(II)−Mn(II) interaction via a superexchange mechanism because the distances between Mn(II)···O···Mn(II) are 2.28(3) and 2.27(3) Å, respectively (Figure 9). The rise below 3 K could be due to the weak ferromagnetic interaction between the Mn(II) ions. $M-H$ curves at all the measured temperature values show linear behavior (Figure 14b).

CONCLUSION

In conclusion, we have described construction of four new coordination polymers under hydro(solvo)thermal conditions. Variable-temperature magnetic studies demonstrate that complex **1** exhibits weak ferromagnetic ordering at low temperature owing to the frustration of one of the Co(II) ions in the unit cell. Complex **2** shows a peak at ~6.1 K in ZFC susceptibility, which might be due to presence of weak ferromagnetic interactions between carboxylate-bridged Co(II) ions. Complex **4** shows maxima at 13 K in both ZFC and FC susceptibility curves, which indicates the occurrence of an antiferromagnetic transition.

ASSOCIATED CONTENT

Supporting Information

X-ray crystallographic data in CIF format, selected bonds and distances for **1**−**4**, complete data for IR, TGA, PXRD measurements, and additional figures. This material is available free of charge via the Internet at http://pubs.acs.org.

AUTHOR INFORMATION

Corresponding Author

*E-mail: pkb@iitk.ac.in.

Notes

The authors declare no competing financial interest.

ACKNOWLEDGMENTS

We gratefully acknowledge the financial support received from the Department of Science and Technology, New Delhi, India (to P.K.B.), and SRF from the CSIR to M. A. NCL authors acknowledge the financial help from the CSIR young scientist award grant.

REFERENCES

(1) (a) Sharma, M. K.; Senkovska, I.; Kaskel, S.; Bharadwaj, P. K. *Inorg. Chem.* **2011**, *50*, 539. (b) Ferey, G. *Chem. Soc. Rev.* **2008**, *37*, 191. (c) Rowsell, J. L. C.; Yaghi, O. M. *Angew. Chem., Int. Ed* **2005**, *44*, 4670. (d) Kitagawa, S.; Kitaura, R.; Noro, S. *Angew. Chem., Int. Ed.* **2004**, *43*, 2334. (e) Das, M. C.; Bharadwaj, P. K. *J. Am. Chem. Soc.* **2009**, *131*, 10942. (f) Ōkawa, H.; Shigematsu, A.; Sadakiyo, M.; Miyagawa, T.; Yoneda, K.; Ohba, M.; Kitagawa, H. *J. Am. Chem. Soc.* **2009**, *131*, 13516. (g) Yamada, T.; Sadakiyo, M.; Kitagawa, H. *J. Am. Chem. Soc.* **2009**, *131*, 3144. (h) Dechambenoit, P.; Long, J. R. *Chem. Soc. Rev.* **2011**, *40*, 3249. (i) Jiang, H.-L.; Xu, Q. *Chem. Commun.* **2011**, *47*, 3351. (j) Chen, Lei.; Xu, G.-J.; Shao, K.-Z.; Zhao, Y.-H.; Yang, G.-S.; Lan, Y.-Q.; Wang, X.-L.; Xu, H.-B.; Su, Z.-M. *CrystEngComm.* **2010**, *12*, 5157. (k) Yang, J.; Song, S.-Y.; Ma, J.-F.; Liu, Y.-Y.; Yu, Z.-T. *Cryst. Growth Des.* **2011**, *11*, 5469. (l) Zhang, X.; Yang, J.-X.; Zhang, J.; Cheng, J.-K.; Sun, M.-L.; Yao, Y.-G. *Inorg. Chem. Commun.* **2011**, *14*, 986.

(2) (a) Hu, B.-W.; Zhao, J.-P; Sañudo, E. C.; Liu, F.-C.; Zeng, Y.-F.; Bu, X.-H. *Dalton Trans.* **2008**, 5556. (b) Duan, Z.; Zhang, Y.; Zhang, B.; Zhu, D. *J. Am. Chem. Soc.* **2009**, *131*, 6934. (c) Prasad, T. K.; Rajasekharan, M. V.; Costes, J.-P. *Angew. Chem., Int. Ed.* **2007**, *46*, 2851. (d) Pachfule, P.; Das, R.; Poddar, P.; Banerjee, R. *Cryst. Growth Des.* **2010**, *10*, 2475.

(3) (a) Yang, E.-C.; Yang, Y.-L.; Liu, Z.-Y.; Liu, K.-S.; Wu, X.-Y.; Zhao, X.-J. *CrystEngComm.* **2011**, *13*, 2667. (b) Lytvynenko, A. S.; Kolotilov, S. V.; Cador, O.; Golhen, S.; Ouahab, L.; Pavlishchuk, V. V. *New J. Chem.* **2011**, *35*, 2179. (c) Kou, H.-Z.; Jiang, Y.-B.; Cui, A.-L. *Cryst. Growth Des.* **2005**, *5*, 77. (d) Yang, E.- C.; Liu, Z.- Y.; Shi, X.- J.; Liang, Q.- Q.; Zhao, X.-J. *Inorg. Chem.* **2010**, *49*, 7969. (e) Ahmad, M.; Sharma, M. K.; Das, R.; Poddar, P.; Bharadwaj, P. K. *Cryst. Growth Des.* **2012**, *12*, 1571.

(4) (a) Zhang, X. X.; Chui, S. S.-Y.; Williams, I. D. *J. Appl. Phys.* **2000**, *87*, 6007. (b) Moulton, B.; Lu, J.; Hajndl, R.; Hariharan, H.; Zaworotko, M. J. *Angew. Chem., Int. Ed.* **2002**, *41*, 2821. (c) Pachfule, P.; Das, R.; Poddar, P.; Banerjee, R. *Cryst. Growth Des.* **2011**, *11*, 1215. (d) Dey, C.; Das, R.; Saha, B. K.; Poddar, P.; Banerjee, R. *Chem. Commun.* **2011**, *47*, 11008.

(5) (a) Zapf, V. S.; Kenzelmann, M. K.; Wolff-Fabris, F.; Balakirev, F.; Chen, Y. *Phys. Rev. B* **2008**, *82*, 1. (b) Pachfule, P.; Das, P.; Poddar, P.; Banerjee, R. *Inorg. Chem.* **2011**, *50*, 3855.

(6) (a) Liu, J.-Q.; Liu, B.; Wang, Y.-Y.; Liu, P.; Yang, G.-P.; Liu, R.-T.; Shi, Q.-Z.; Batten, S. R. *Inorg. Chem.* **2010**, *49*, 10422. (b) Halder, G. J.; Kepert, C. J.; Moubaraki, B.; Murray, K. S.; Cashion, J. D. *Science* **2002**, *298*, 1762.

(7) (a) Xu, N.; Shi, W.; Liao, D.-Z.; Yan, S.-P.; Cheng, P. *Inorg. Chem.* **2008**, *47*, 8748. (b) Kurmoo, M.; Kumagai, H.; Chapmanc, K. W.; Kepert, C. J. *Chem. Commun.* **2005**, 3012.

(8) (a) Aijaz, A.; Sañudo, E. C.; Bharadwaj, P. K. *Inorg. Chem. Acta* **2009**, *362*, 4246. (b) Zheng, Y.-Z.; Xue, W.; Tong, M.-L.; g Chen, X.-M.; Grandjean, F.; Long, G. J. *Inorg. Chem.* **2008**, *47*, 4077.

(9) (a) Lama, P.; Aijaz, A.; Sañudo, E. C.; Bharadwaj, P. K. *Cryst. Growth Des.* **2010**, *10*, 283. (b) Zeng, M.-H.; Zhang, W.-Z.; Sun, X.-Z.; Chen, X.-M. *Angew. Chem., Int. Ed.* **2005**, *44*, 3079. (c) Lama, P.; Aijaz, A.; Sañudo, E. C.; Bharadwaj, P. K. *Dalton Trans.* **2012**, *41*, 2979.

(10) (a) Wang, Y.-Q.; Sun, W.-W.; Wang, Z.-D.; Jia, Q.-X.; Gao, E.-Q.; Song, Y. *Chem.Commun.* **2011**, 6386. (b) Miyasaka, H.; Julve, M.; Yamashita, M.; Clerac, R. *Inorg. Chem.* **2009**, *48*, 3420. (c) Brockman, J. T.; Stamatatos, T. C.; Wernsdorfer, W.; Abboud, K. A.; Christou, G. *Inorg. Chem.* **2007**, *46*, 9160. (d) Oullette, W.; Prosvirin, A. V.; Whitenack, K.; Dunbar, K. R.; Zubieta, J. *Angew. Chem., Int. Ed.* **2009**, *48*, 2140.

(11) Tran, V. H.; Świątek-Tran, B. *Dalton Trans.* **2008**, 4860.

(12) (a) Jain, P.; Ramachandran, V.; Clark, R. J.; Zhou, H. D.; Toby, B. H.; Dalal, N. S.; Kroto, H. W.; Cheetham, A. K. *J. Am. Chem. Soc.* **2009**, *131*, 13625. (b) Cui, H.; Zhou, B.; Long, L. S.; Okano, Y.; Kobayashi, H.; Kobayashi, A. *Angew. Chem., Int. Ed.* **2008**, *47*, 3376. (c) Cui, H. B.; Wang, Z. M.; Takahashi, k.; Okano, Y.; Kobayashi, H.; Kobayashi, A. *J. Am. Chem. Soc.* **2006**, *128*, 15074. (c) Stroppa, A.; Jain, P.; Barone, P.; Marsman, M.; Perez-Mato, J. M.; Cheetham, A. K.; Kroto, H. W.; Picozzi, S. *Angew. Chem., Int. Ed.* **2011**, *50*, 5847.

(13) (a) Chen, W.-X.; Zhuang, G.-L.; Zhao, H.-X.; Long, L.-S.; Huang, R.-B.; Zheng, L.-S. *Dalton Trans.* **2011**, *40*, 10237. (b) Sun, Q.; Cheng, A.-l.; Wang, Y.-Q.; Ma, Y.; Gao, E.-Q. *Inorg. Chem.* **2011**, *50*, 8144. (c) Zheng, Y.-Q.; Lin, J.-L.; Kong, Z.-P. *Inorg. Chem.* **2004**, *43*, 2590.

(14) (a) Lama, P.; Mrozinski, J.; Bharadwaj, P. K. *Cryst. Growth Des.* **2012**, *12*, 3158. (b) Lu, W.-G.; Jiang, L.; Feng, X.-L.; Lu, T.-B. *Cryst. Growth Des.* **2006**, *6*, 564. (c) Lü, X.-Q.; Jiang, J.-J.; Chen, C.-L.; Kang, B.-S.; Su, C.-Y. *Inorg. Chem.* **2005**, *44*, 4515.

(15) König, E. *Magnetic Properties of Coordination and Organometallic Transition Metal Compounds*; Springer: Berlin, 1966.
(16) *International Tables for X-Ray Crystallography*; Kynoch Press: Birmingham, England, 1952; Vol. *III*.
(17) SAINT, version 6.02; Bruker AXS: Madison, WI, 1999.
(18) Sheldrick, G. M. *SADABS: Empirical Absorption Correction Program*; University of Göttingen: Göttingen, Germany, 1997.
(19) XPREP, version 5.1; Siemens Industrial Automation Inc.; Madison, WI, 1995.
(20) Sheldrick, G. M. *SHELXTL Reference Manual*, version 5.1; Bruker AXS: Madison, WI, 1997.
(21) Sheldrick, G. M.; *SHELXL-97: Program for Crystal Structure Refinement*; University of Göttingen: Göttingen, Germany, 1997.
(22) (a) Collman, J. P.; Brauman, J. I.; Fitzgerald, J. P.; Hampton, P. D.; Naruta, Y.; Sparapany, J. W.; Ibers, J. A. *J. Am. Chem. Soc.* **1988**, *110*, 3477. (b) Niu, Y.; Hou, H.; Wei, Y.; Fan, Y.; Zhu, Y.; Du, C.; Xin, X. *Inorg. Chem. Commun.* **2001**, *4*, 358.
(23) (a) Lisnard, L.; Mialane, P.; Dolbecq, A.; Marrot, J.; Clemente-Juan, J. M.; Coronado, E.; Keita, B.; de Oliveira, P.; Nadjo, L.; Secheresse, F. *Chem.—Eur. J.* **2007**, *13*, 3525. (b) Li, X.-J.; Wang, X.-Y.; Gao, S.; Cao, R. *Inorg. Chem.* **2006**, *45*, 1508.
(24) See Supporting Information.
(25) (a) Tang, Y.-Z.; Wang, X.-S.; Zhou, T.; Xiong, R.-G. *Cryst. Growth Des.* **2006**, *6*, 11. (b) Dobrzynska, D.; Jerzykiewicz, L. B.; Jezierska, J.; Duczmal, M. *Cryst. Growth Des.* **2005**, *5*, 1945.
(26) (a) Lama, P.; Aijaz, A.; Sañudo, E. C.; Bharadwaj, P. K. *Cryst. Growth Des.* **2010**, *10*, 283. (b) Lee, E. W.; Kim, Y. J.; Jung, D.-Y. *Inorg. Chem.* **2002**, *41*, 501.
(27) (a) Tang, Y.-Z.; Wang, X.-S.; Zhou, T.; Xiong, R. G. *Cryst. Growth Des.* **2006**, *6*, 11. (b) Tian, C. B.; He, Z. Z.; Li, Z. H.; Lin, P.; Du, S. W. *CrystEngComm* **2011**, *13*, 3080. (c) Li, W.; Jia, H. P.; Ju, Z. F.; Zhang, J. *Dalton Trans.* **2008**, 5350.
(28) (a) The network topology was evaluated by the program "TOPOS-4.0", see: http://www.topos.ssu.samara.ru. Blatov, V. A. *IUCr CompComm. Newsl.* **2006**, *7*, 4. (b) Blatov, V. A.; Shevchenko, A. P.; Serezhkin, V. N. *J. Appl. Crystallogr.* **2000**, *33*, 1193. (c) Blatov, V. A.; O'Keeffe, M.; Proserpio, D. M. *CrystEngComm* **2010**, *12*, 44.